Theoretical Study on Exciton Recurrence Motion in Anthracene Dimer Using the Ab Initio MO-CI Based Quantum Master Equation Approach

Ryohei Kishi,* Masayoshi Nakano,* Takuya Minami, Hitoshi Fukui, Hiroshi Nagai, Kyohei Yoneda, and Hideaki Takahashi

Department of Materials Engineering Science, Graduate School of Engineering Science, Osaka University, Toyonaka, Osaka 560-8531, Japan

Received: December 17, 2008; Revised Manuscript Received: February 26, 2009

We apply the ab initio molecular orbital (MO)-configuration interaction (CI) based quantum master equation (MOQME) method to the investigation of ultrafast exciton dynamics in an anthracene dimer modeled after anthracenophane, which is experimentally found to exhibit an oscillatory signal of fluorescence anisotropy decay. Two low-lying near-degenerate one-photon allowed excited states with a slight energy difference (42 cm^{-1}) are obtained at the CIS/6-31G** level of approximation using full valence π-orbitals. The time evolution of reduced exciton density matrices is performed by numerically solving the quantum master equation. After the creation of a superposition state of these near-degenerate states by irradiating a near-resonant laser field, we observe two kinds of oscillatory behaviors of polarizations: field-induced polarizations with faster periods, and amplitude oscillations of *x*- and *z*-polarizations, P^x and P^z, with a slower period, in which the amplitudes of P^x and P^z attain maximum alternately. The latter behavior turns out to be associated with an oscillatory exciton motion between the two monomers, i.e., exciton recurrence motion, using the dynamic exciton expression based on the polarization density. From the analysis of contribution to the exciton distributions, such exciton recurrence motion is found to be characterized by both the difference in eigenfrequencies between the two near-degenerate states excited by the laser field and the relative phases among the frontier MOs primarily contributing to the near-degenerate states.

1. Introduction

Coherent and incoherent (relaxation) dynamics of exciton (electron−hole pair) in molecular aggregates and supermolecular systems is one of the recent hot topics in view of a fundamental understanding of dynamical quantum phenomena in biological systems as well as in photonics and optoelectronics systems.[1−34] Exciton migration[6−24] and exciton recurrence motion,[25−34] e.g., coherent energy transfer[25,26] and oscillatory fluorescence anisotropy of two chromophores,[28−32] have been intensely investigated both experimentally and theoretically. The relaxation theory[35] based on the reduced system density matrix formula is widely used to describe various relaxation phenomena, originating in the coupling with surrounding quantum systems, in combination with the molecular aggregate models, e.g., Frenkel exciton model,[36] in which a pair of electron and hole moves under a constraint of taking the same position with each other and of prohibiting the exchange between electrons (holes) at different positions.

In experiments, several energy transfer dynamics between choromophores can be observed by the fluorescence anisotropy ratio, $r(t) = \{I_{||}(t) - I_{\perp}(t)\}/\{I_{||}(t) + 2I_{\perp}(t)\}$, where $I_{||}$ and $I_{\perp}$ are polarization components of signals parallel and perpendicular to the polarization direction of the excitation light, respectively. When linear polarized light is applied to the sample, choromophores whose transition moment is parallel to the polarization plane will be excited selectively. Fluorescence from the excited chromophores is depolarized for several reasons, such as, difference of transition moment vector between the absorption and emission processes, rotation motion of the chromophore, and energy transfer to another chromophore. For bichromophore systems, if excitonic coupling β of the two chromophores is *weak* or *intermediate* regeon (10−50 cm^{-1}), the excited energy level splits with gap of 2β. One can create a superposition state of these two excited states with the use of, for example, uncertainty-principle limited pulse. From the analysis with the localized (Frenkel) exciton model, one has oscillatory solution of the exciton density between the two chromophores with time period of $h/2\beta$.[30,31] In general, such superposition state is collapsed immediately by several dephasing processes. Therefore, oscillatory fluorescence anisotoropy related to the oscillation of excitation will be observed, at least, under the following conditions: (i) transition moments of the two chromophores should be nonparalell (hopefuly almost perpendicular to each other), and (ii) the dephasing time scale should be long enough to observe the oscillatory behavior clearly. One strategy to satisfy these conditions is to bridge two chromophores by linker parts.[30,31]

Yamazaki and co-workers have found that several types of anthracene dimers exhibit damped oscillations of fluorescence anisotropy decay with periods of around 1 ps.[30−32] They have estimated the intermonomer electronic coupling and decay time using the optical Bloch equation based on the Frenkel exciton approach. For example, 1.0 and 1.2 ps of oscillation period and dephasing time are estimated in 2,15-dithia[3,3](1,5)anthracenophane (DTA) in THF solution, respectively.[30,31] This treatment can describe the mechanism of exciton dynamics in molecular aggregates with weak interactions, e.g., van der Waals (dipole−dipole) interactions. It is, however, known that such treatment fails to describe

* Corresponding authors. Tel: +81-6-6850-6265. Fax: +81-6-6850-6268. E-mails: rkishi@cheng.es.osaka-u.ac.jp (R.K.), mnaka@cheng.es.osaka-u.ac.jp (M.N.).

10.1021/jp8111588 CCC: $40.75
Published on Web 03/30/2009

exciton dynamics in aggregates with strong interactions, e.g., charge transfer interactions, and in supermolecular systems with extended exciton delocalization.

To address these issues and to clarify the real microscopic dynamical behavior of electron and hole density distributions, we have proposed a quantum master equation approach combined with the ab initio molecular orbital (MO)-configuration interaction (CI) method, referred to as the MOQME approach.[14] The MOQME approach has succeeded in describing incoherent dynamics, e.g., unidirectional exciton migration in phenylacetylene nanostar dendrimers,[24] in which the relaxation mechanism is analyzed in view of frontier MO interactions. More recently, we have extended this approach by defining a novel dynamic exciton expression reproducing the dynamic polarization, which can describe the coherent dynamics in addition to the incoherent dynamics.[37] As an example, we have applied the dynamic exciton expression to the Rabi oscillation in H_2 molecule and have obtained the spatiotemporal evolution picture of electron and hole density distributions for the field-induced dynamic polarizations.[37] In this study, we therefore apply this appraoch to the investigation of coherent dynamics, i.e., exciton recurrence motion, in an anthracene dimer mimicking realistic DTA from the viewpoint of the microscopic dynamical behaviors of spatial electron and hole density distributions, which cannot be elucidated by the conventional aggregate model approaches.

2. MOQME Approach

We briefly explain the MOQME approach because its details are provided in previous papers.[14,24,37] The reduced exciton density matrices in the singlet adiabatic exciton state basis $\{|\alpha\rangle(\equiv|^1\Psi_\alpha\rangle)\}$ are employed:

$$|\alpha\rangle = \sum_i^N |i\rangle\langle i|\alpha\rangle = \sum_i^N |i\rangle C_{i\alpha} \tag{1}$$

Here, $\{|i\rangle(\equiv|^1\Psi_a^r\rangle)\}$ represent the singly excitation configurations from occupied (a) to virtual (r) MO, which are assumed to compose the one-exciton bases and the vacuum [Hartree−Fock (HF) ground] state $|1\rangle$. The expansion coefficients, $\{C_{i\alpha}\}$ (referred to as CI coefficients), are obtained by the ab initio singly excitation CI (CIS) calculation using the Gaussian 03 program package.[38]

Assuming the weak interaction between exciton and phonon bath states, we derive the quantum master equation [in the atomic units ($\hbar = e = m = 1$)] for the reduced system density matrices $\{\rho_{\alpha\beta}\}$ in the Born−Markov approximation:[23,24]

$$\frac{d\rho_{\alpha\alpha}}{dt} = -\sum_\beta^M \Gamma_{\alpha\alpha;\beta\beta}\rho_{\beta\beta} - F^l \sum_\beta^M (\mu^l_{\alpha\beta}\rho_{\beta\alpha} - \rho_{\alpha\beta}\mu^l_{\beta\alpha}) \tag{2}$$

and

$$\frac{d\rho_{\alpha\beta}}{dt} = -i(\omega_\alpha - \omega_\beta)\rho_{\alpha\beta} - \sum_{\gamma\delta}^M \Gamma_{\alpha\beta;\gamma\delta}\rho_{\gamma\delta} - F^l \sum_\gamma^M (\mu^l_{\alpha\gamma}\rho_{\gamma\beta} - \rho_{\alpha\gamma}\mu^l_{\gamma\beta}) \tag{3}$$

Here, M indicates the number of electronic states involving the ground and excited states used in the MOQME approach, F^l is a laser amplitude in the l-direction, and $\mu^l_{\alpha\beta}$ indicates the lth component of transition moment between states α and β. The first term on the right-hand side of eq 2 and the second term on the right-hand side of eq 3 represent relaxation terms characterized by the relaxation parameters Γ (see refs 23 and 37 for details).

The system density matrices $\{\rho_{\alpha\beta}\}$ obtained by numerically solving eqs 2 and 3 are converted to $\{\rho^{ex}_{ij}\}$ in the one-exciton basis using $\rho^{ex}_{ij}(t) = \sum_{\alpha\beta}^M C^*_{i\alpha}C_{j\beta}\rho_{\alpha\beta}(t)$. The time evolution of system polarization $P^l(t)$ is calculated by

$$P^l(t) \equiv \mathrm{tr}[\mu^l\rho(t)] = \int \rho_{\mathrm{pol}}(\mathbf{r},t)(-r^l)\,d\mathbf{r} \tag{4}$$

Here, $\rho_{\mathrm{pol}}(\mathbf{r},t)$ is the polarization density defined by the density difference between the reduced one-electron density $[\rho(\mathbf{r},t)]$ at time t and that $[d_{11}(\mathbf{r})]$ at the initial time, that is,

$$\rho_{\mathrm{pol}}(\mathbf{r},t) \equiv \rho(\mathbf{r},t) - d_{11}(\mathbf{r}) = \sum_{i=2}[d_{ii}(\mathbf{r}) - d_{11}(\mathbf{r})]\rho_{ii}(t) + 2\sum_{i=2} d_{1i}(\mathbf{r})\rho^{\mathrm{real}}_{1i}(t) + 2\sum_{i<j(i,j\neq 1)} d_{ij}(\mathbf{r})\rho^{\mathrm{real}}_{ij}(t) \tag{5}$$

where $\{d_{ij}(\mathbf{r})\}$ indicate the reduced one-electron density matrices in the one-exciton basis $\{|i\rangle\}$ including the HF ground state $|1\rangle$, and $\{\rho^{\mathrm{ex\ real}}_{ij}(t)\}$ represent the real parts of system density matrices in the one-exciton basis. Using the occupied $\{\psi_a(\mathbf{r}), \psi_b(\mathbf{r}),...\}$ and virtual $\{\psi_r(\mathbf{r}), \psi_s(\mathbf{r}),...\}$ MOs, eq 5 can be evaluated by

$$\rho_{\mathrm{pol}}(\mathbf{r},t) = \sum_{i=2}[|\psi_r(\mathbf{r})|^2 - |\psi_a(\mathbf{r})|^2]\rho^{\mathrm{ex}}_{ii}(t) + 2\sum_{i(a\to r)=2}\sqrt{2}\psi_a(\mathbf{r})\,\psi_r(\mathbf{r})\rho^{\mathrm{ex\ real}}_{1i}(t) + 2\sum_{\substack{i(a\to r)\\ <j(a\to s)\\ (i,j\neq 1)}}\psi_r(\mathbf{r})\,\psi_s(\mathbf{r})\rho^{\mathrm{ex\ real}}_{ij}(t) - 2\sum_{\substack{i(a\to r)\\ <j(b\to r)\\ (i,j\neq 1)}}\psi_a(\mathbf{r})\,\psi_b(\mathbf{r})\rho^{\mathrm{ex\ real}}_{ij}(t) \tag{6}$$

We can appropriately define the relationship between the polarization density and the electron and hole densities by $\rho_{\mathrm{pol}}(\mathbf{r},t) \equiv \rho_{\mathrm{elec}}(\mathbf{r},t) - \rho_{\mathrm{hole}}(\mathbf{r},t)$, which implies that the deviation of the electron distribution from the hole distribution gives the polarization density. Thus, we define the expressions of $\rho_{\mathrm{elec}}(\mathbf{r},t)$ and $\rho_{\mathrm{hole}}(\mathbf{r},t)$ as[37]

$$\rho_{\mathrm{elec}}(\mathbf{r},t) = \sum_{i(a\to r)=2}[\rho^{\mathrm{ex}}_{ii}(t)|\psi_r(\mathbf{r})|^2 + \sqrt{2}\psi_a(\mathbf{r})\,\psi_r(\mathbf{r})\rho^{\mathrm{ex\ real}}_{1i}(t) + 2\sum_{j(a\to s)(>i)}\psi_r(\mathbf{r})\,\psi_s(\mathbf{r})\rho^{\mathrm{ex\ real}}_{ij}(t)] \tag{7}$$

and

$$\rho_{\mathrm{hole}}(\mathbf{r},t) = \sum_{i(a\to r)=2}[\rho^{\mathrm{ex}}_{ii}(t)|\psi_a(\mathbf{r})|^2 - \sqrt{2}\psi_a(\mathbf{r})\,\psi_r(\mathbf{r})\rho^{\mathrm{ex\ real}}_{1i}(t) + 2\sum_{j(b\to r)(>i)}\psi_a(\mathbf{r})\,\psi_b(\mathbf{r})\rho^{\mathrm{ex\ real}}_{ij}(t)] \tag{8}$$

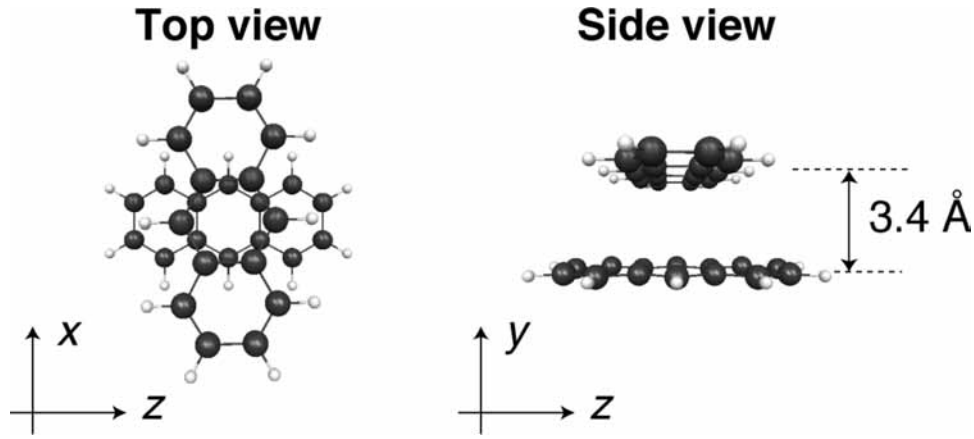

Figure 1. Top ($z-x$ plane) and side ($z-y$ plane) views of structure of anthracene dimer, in which the monomer geometry is optimized by the B3LYP/6-31G** method. The two anthracene molecules are arranged in a face-to-face stack form with a rotational angle of 88.5° and an intermolecular distance of 3.4 Å.

TABLE 1: Excitation Energies E (cm^{-1}) and l-Axis Components of Transition Moments from the Ground State μ^l (D) for the First and Second Excited States

state	E (cm^{-1})	μ^x (D)	μ^y (D)	μ^z (D)	main configuration (CI coefficient)[a]
2	36 591	1.38	0.00	−1.42	H→L (0.743), H−1→L+1 (−0.523)
3	36 633	−1.46	0.00	−1.42	H−1→L (0.725), H→L+1 (−0.552)

[a] H and L denote HOMO and LUMO, respectively.

3. Structure and Exciton States of Model Dimer

Figure 1 shows the structure of the anthracene dimer model, in which the monomer geometry is optimized by the B3LYP/6-31G** method. The two anthracene monomers are arranged in a face-to-face stack form with a rotational angle of 88.5° and an intermolecular distance of 3.4 Å, which are taken from the experimental data in refs 30 and 31. The longitudinal axis of the lower side molecule is set to be parallel to the z-axis. We obtain 20 excited states calculated by the CIS/6-31G** method using full valence π-orbitals. All quantum chemical calculations and the generation of three-dimensional (3D) grid data of MOs are performed by the Gaussian03 program package.[38]

Table 1 summarizes the calculated excitation energies, transition moments, and CI coefficients of the lowest two excited states **2** and **3** for the dimer system. The frontier MOs for the dimer are shown in Figure 2. The dominant excitation configurations of the two excited states are HOMO→LUMO and HOMO−1→LUMO+1 for state **2**, and HOMO−1→LUMO and HOMO→LUMO+1 for state **3**. These four frontier MOs are made by symmetric and antisymmetric mixings of HOMO and LUMO of the monomer. It is known that the anthracene monomer possesses a latitudinal component of the transition moment between the ground and first excited states. Because the transition dipole directions of the two anthracene monomers are almost perpendicular to each other, the electronic coupling between the monomers in the excited state is predicted to be very weak. Although the CIS excitation energies are known to overshoot the experimental values, the energy difference of 42 cm^{-1} between near-degenerate states **2** and **3** is found to be comparable to that estimated from the experiment in DTA (28.6 cm^{-1}).[30,31]

Using transition energies and moments, the exciton dynamics is performed by numerically solving eqs 2 and 3 with the sixth-order Runge−Kutta method. We focus on the exciton recurrence motion in this system, the relaxation (population damping and dephasing) terms are not considered. We first apply the external continuous wave (cw) laser field with the x-polarization direction, $\mathbf{F}(t) = F^x \cos \omega t$. The field frequency $\omega = 36\,612$ cm^{-1} [$=(\omega_2 + \omega_3)/2$] is chosen to create a superposition state of states **2** and **3**. The field power is set to 10^3 MW/cm^2, which is strong enough to populate both the target states creating the superposition state. One optical cycle is about 0.911 fs and after 200 optical cycles (∼182 fs), the laser field is cut off. The time evolution of exciton density matrices is performed until 3000 optical cycles ∼2.7 ps).

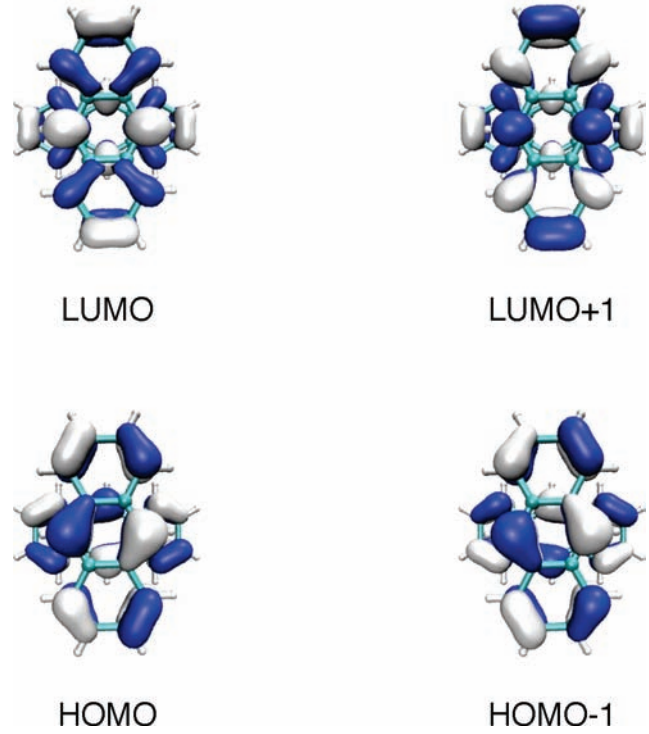

Figure 2. Isosurface maps [blue (+) and white (−) contours with an amplitude of 0.03 au] of HOMO−1, HOMO, LUMO, LUMO+1 of the anthracene dimer model calculated at the HF/6-31G** level of approximation.

4. Exciton Dynamics in Model Dimer

Figure 3a shows the exciton population dynamics of states **2** and **3**. It is found that exciton is populated in these two states, so that a superposition state is created. Figure 3b shows the x-

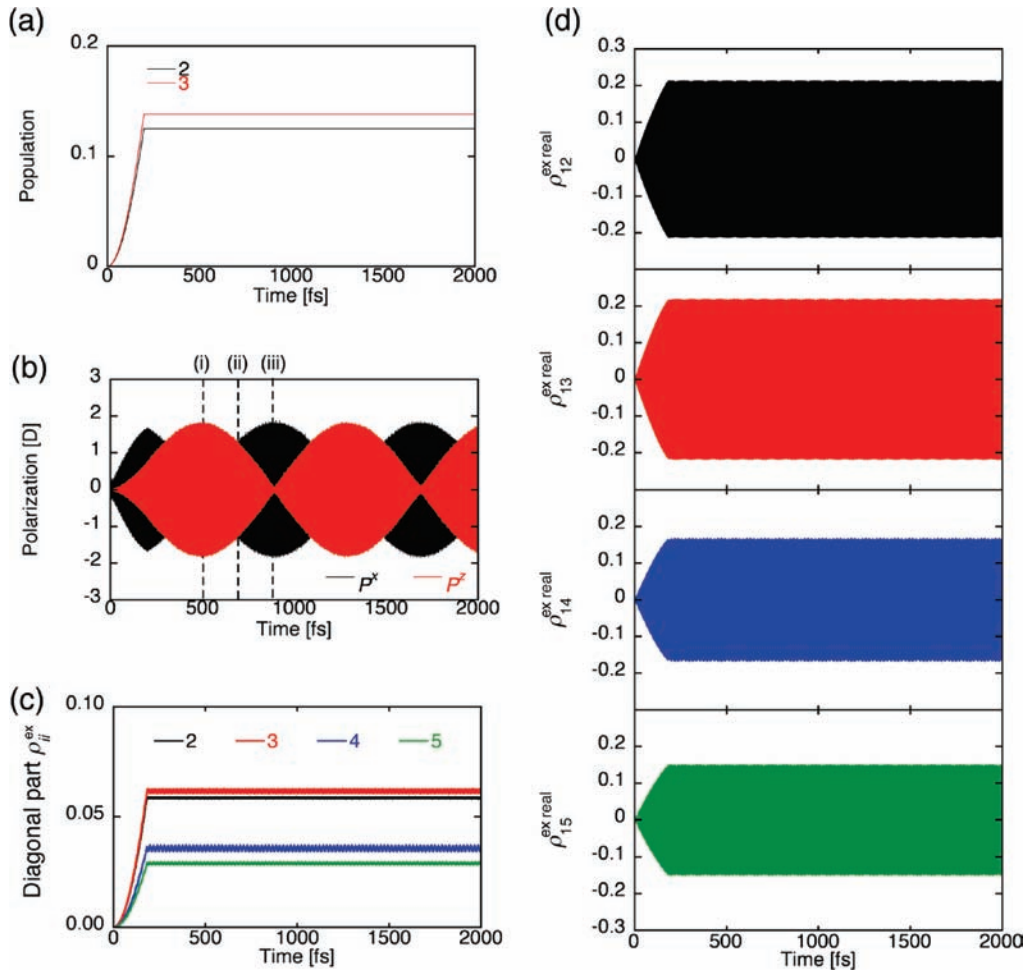

Figure 3. Time evolution of exciton population of states **2** and **3** (a), *x*- and *z*-axis components of system polarization P^x and P^z (b), and diagonal $[\rho_{ii}^{ex}(t)]$ (c) and off-diagonal $[\rho_{1i}^{ex\ real}(t)]$ (d) density matrices for singly excitation configurations, $i = 2$ (HOMO→LUMO), 3 (HOMO−1→LUMO), 4 (HOMO→LUMO+1), and 5 (HOMO−1→LUMO+1).

and *z*-polarizations, P^x and P^z, calculated by $P^l(t) = \mathrm{Tr}[\mu^l \rho(t)]$. In the induction period until cutting off the laser field ($t < 182$ fs), the *x*-polarization is induced by the interaction with the external field. Subsequently, the increase of *z*-polarization amplitudes is also observed. Even after cutting off the field, the oscillations of population and polarization are shown to remain without decay owing to the neglect of relaxation terms. The rapid oscillations of field-induced polarizations P^x and P^z turn out to be consistent with the oscillation of the applied laser field. We can also observe the long period of oscillations of polarization amplitudes. The period of such long time oscillation of P^x (or P^z) amplitude is estimated to be about 0.8 ps. After cutting off the field ($t > 182$ fs), it is found that the maximum amplitudes of P^x and P^z are observed alternately: when the amplitude of P^z attains the maximum, P^x exhibits a negligible amplitude, and vice versa. Such alternation of the amplitudes of P^x and P^z corresponds to the oscillatory behavior of fluorescence anisotropy decay in the experiments, i.e., damped exciton recurrence motion between the two monomers. Indeed, an oscillation period of 0.8 ps is found to be comparable to the experimental characteristic oscillation time of fluorescence anisotropy signal for DTA (∼1.0 ps). Figure 3c shows the time evolution of diagonal exciton density matrices, $\rho_{ii}^{ex}(t)$, in the one-exciton basis, where $i = 2-5$ correspond to the excitation configurations, HOMO→LUMO, HOMO−1→LUMO, HOMO→LUMO+1, and HOMO−1→LUMO+1, respectively. These configurations are found to primarily contribute to exciton states **2** and **3** (see Table 1). Contrary to the previous result using the dipole-coupled Frenkel exciton model,[33,34] we cannot observe the oscillatory behaviors of $\rho_{ii}^{ex}(t)$ relating to the exciton recurrence motion. Moreover, the off-diagonal density matrices $\rho_{1i}^{ex\ real}(t)$ shown in Figure 3d exhibit rapid oscillations induced by the oscillating external electric field. The reason why the calculated polarizations show slower oscillations of amplitudes is discussed in detail in section 5.

We compute 3D grid data of exciton density distributions using eqs 7 and 8 at times (i)−(iii) shown in Figure 3b: at time (i) (around 501 fs) P^z exhibits a maximum amplitude, and $P^x \sim 0$, at time (ii) (around 692 fs) P^z and P^x exhibit similar amplitude, and at time (iii) (around 893 fs) P^x exhibits a maximum amplitude, and $P^z \sim 0$. Parts a−c of Figure 4 show the snapshots of exciton density distributions in one optical cycle at times (i), (ii), and (iii), respectively. The left, center, and right snapshots in one optical cycle around each time show the exciton density distributions around three phases, $2\pi n$, $\pi/2 + 2\pi n$, and $\pi + 2\pi n$ (n: integer), respectively. At time (i) (Figure 4a), the electron and hole densities are shown to be distributed mainly on the upper side molecule, and to oscillate asymmetrically in the *z*-direction, leading to P^z. After time (i), the amplitude of P^z decreases gradually, and that of P^x grows [see Figure 3b (i) and (ii)]. In the intermediate stage at time (ii), the exciton appears on both monomers (see Figure 4b). Within the upper and lower side molecules, asymmetric oscillations of electron and hole densities are observed along the *z*- and *x*-axes, which

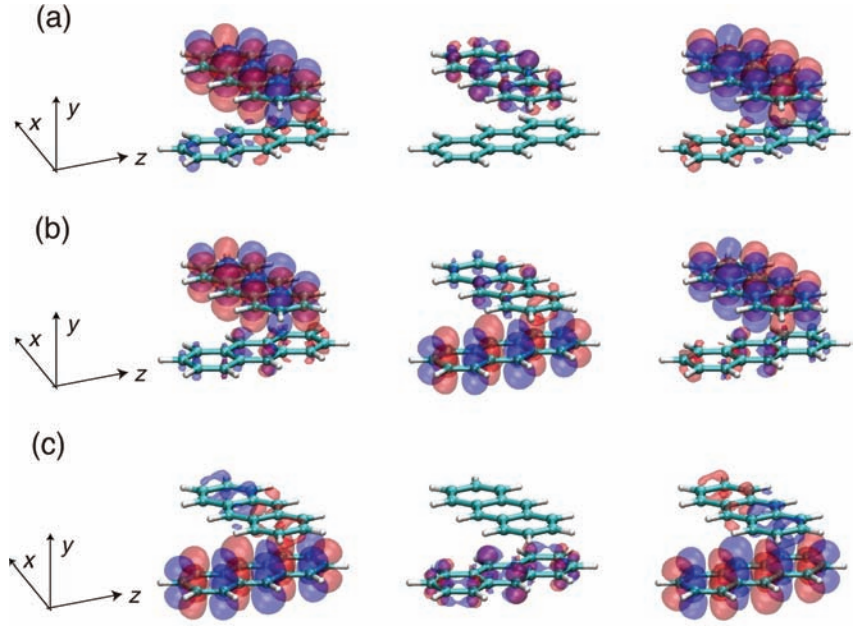

Figure 4. Snapshots of electron and hole densities calculated by eqs 7 and 8 in one optical cycle around $t \sim 501$ fs (a), $t \sim 692$ fs (b), and $t \sim 893$ fs (c). The left, center, and right snapshots in one optical cycle around each time show the exciton density distributions around three phases, $2\pi n$, $\pi/2 + 2\pi n$, and $\pi + 2\pi n$ (n: integer), respectively. Red and blue isosurfaces represent electron and hole density maps with contour values of 0.001 au, respectively.

are the origins of P^z and P^x, respectively. After time (ii), the amplitude of P^z disappears, whereas that of P^x attains a maximum at time (iii), where the electron and hole densities are observed mainly on the lower side molecule, and are shown to oscillate along the x-axis. These results indicate the dynamical behavior of spatial electron and hole density distributions for the exciton recurrence motion between the anthracene monomers with a period of ~0.8 ps.

5. Mechanism of Exciton Recurrence Motion

To elucidate why the slow oscillations of polarization amplitudes appear, we investigate the contribution of each term appearing in eq 5 in the present model. This also enables us to illuminate the difference in the time evolution of density matrices between the Frenkel exciton and the MOQME approaches. From the definition of polarization density (eq 5) as well as of electron and hole densities (eqs 7 and 8), the second term on the right-hand side of eq 5, $\rho_{1i}^{\text{ex real}}(t)d_{1i}(\mathbf{r})$, contributes dominantly to the oscillatory behavior of exciton because the off-diagonal density matrices here represent the polarizations which originate in the interaction between the external electric field and the transition dipoles associated with the excitation from the ground to the excited states. The $\rho_{1i}^{\text{ex real}}(t)d_{1i}(\mathbf{r})$ is composed of off-diagonal density matrices, $\rho_{1i}^{\text{ex real}}(t)$, in the exciton basis, and the reduced one-electron density matrices, $d_{1i}(\mathbf{r})$ [$=2^{1/2}\psi_a(\mathbf{r})\ \psi_r(\mathbf{r})$]. We therefore analyze the dynamical behavior of polarization by considering the temporal features of $\rho_{1i}^{\text{ex real}}(t)$ and the spatial shapes of $d_{1i}(\mathbf{r})$.

We first investigate the off-diagonal density matrices $\rho_{1i}^{\text{ex real}}(t)$. Parts a−c of Figure 5 show the time evolution of $\rho_{1i}^{\text{ex real}}(t)$ ($i = 2-5$) at times (i), (ii), and (iii), respectively. Each $\rho_{1i}^{\text{ex real}}(t)$ shows rapid oscillatory behavior owing to the oscillating applied electric field (see also Figure 3d). It is noted, however, that not all these terms oscillate in the same phase. It is found at time (i) (Figure 5a) that $\rho_{12}^{\text{ex real}}(t)$ and $\rho_{13}^{\text{ex real}}(t)$ [$\rho_{14}^{\text{ex real}}(t)$ and $\rho_{15}^{\text{ex real}}(t)$] oscillate in phase, whereas $\rho_{12}^{\text{ex real}}(t)$ and $\rho_{14}^{\text{ex real}}(t)$ [$\rho_{13}^{\text{ex real}}(t)$ and $\rho_{15}^{\text{ex real}}(t)$] oscillate in opposite phase. The relative phase between $\rho_{12}^{\text{ex real}}(t)$ and $\rho_{13}^{\text{ex real}}(t)$ [$\rho_{14}^{\text{ex real}}(t)$ and $\rho_{15}^{\text{ex real}}(t)$] turns out to shift gradually with time (see Figure 5b). It is thus shown at time (iii) (Figure 5c) that $\rho_{12}^{\text{ex real}}(t)$ and $\rho_{13}^{\text{ex real}}(t)$ [$\rho_{14}^{\text{ex real}}(t)$ and $\rho_{15}^{\text{ex real}}(t)$] oscillate in opposite phase, whereas $\rho_{12}^{\text{ex real}}(t)$ and $\rho_{14}^{\text{ex real}}(t)$ [$\rho_{13}^{\text{ex real}}(t)$ and $\rho_{15}^{\text{ex real}}(t)$] oscillate in phase, the feature of which is opposite to that at time (i). Additionally, the oscillations of $\rho_{12}^{\text{ex real}}(t)$ and $\rho_{15}^{\text{ex real}}(t)$ [$\rho_{13}^{\text{ex real}}(t)$ and $\rho_{14}^{\text{ex real}}(t)$] show almost mutually opposite phase at any time but with the same frequency. These features can be explained by the difference in eigenfrequencies of the two superposition states. The $\rho_{12}^{\text{ex real}}(t)$ and $\rho_{15}^{\text{ex real}}(t)$ [$\rho_{13}^{\text{ex real}}(t)$ and $\rho_{14}^{\text{ex real}}(t)$] are dominated by the main configurations i=2(HOMO→LUMO) and 5(HOMO−1→LUMO+1) of state **2** [i=3(HOMO−1→LUMO) and 4(HOMO→LUMO+1) of state **3**], which possess positive and negative CI coefficients, respectively (see Table 1). Because the applied field frequency is chosen to be near resonant to these two near-degenerate excited states, the contributions from higher-lying states oscillating with different eigenfrequencies are negligible. Therefore, $\rho_{12}^{\text{ex real}}(t)$ and $\rho_{15}^{\text{ex real}}(t)$ [$\rho_{13}^{\text{ex real}}(t)$ and $\rho_{14}^{\text{ex real}}(t)$] oscillate with the same eigenfrequency of state **2** (state **3**) (see also Table 1). The slight difference in the eigenfrequencies between states **2** and **3** (42 cm^{-1}) is predicted to cause the shift of relative phases of $\rho_{1i}^{\text{ex real}}(t)$ oscillations. Indeed, $\rho_{12}^{\text{ex real}}(t)$ [$\rho_{15}^{\text{ex real}}(t)$] and $\rho_{13}^{\text{ex real}}(t)$ [$\rho_{14}^{\text{ex real}}(t)$] oscillations are shown to be synchronized with each other every ~0.8 ps after time (i), the period of which is consistent with the difference in the eigenfrequencies between states **2** and **3**.

Second, we examine another important contribution, spatial features of $d_{1i}(\mathbf{r})$. Figure 6 shows the isosurface maps of reduced one-electron density matrices $d_{1i}(\mathbf{r})$ [$=2^{1/2}\psi_a(\mathbf{r})\psi_r(\mathbf{r})$] appearing in eq 5. The spatial distributions of $d_{12}(\mathbf{r})$ [$=2^{1/2}\psi_{\text{H}}(\mathbf{r})\ \psi_{\text{L}}(\mathbf{r})$] and $d_{15}(\mathbf{r})$ [$=2^{1/2}\psi_{\text{H}-1}(\mathbf{r})\ \psi_{\text{L}+1}(\mathbf{r})$] are shown to be almost in mutually opposite phase. However, $\rho_{12}^{\text{ex real}}(t)$ and $\rho_{15}^{\text{ex real}}(t)$ are found to oscillate always in opposite phase (see Figure 5), so that the spatial features of $\rho_{12}^{\text{ex real}}(t)d_{12}(\mathbf{r})$ and $\rho_{15}^{\text{ex real}}(t)d_{15}(\mathbf{r})$ are predicted to be very similar to each other at any times. Similar relationship is observed between $\rho_{13}^{\text{ex real}}(t)d_{13}(\mathbf{r})$ and $\rho_{14}^{\text{ex real}}(t)d_{14}(\mathbf{r})$.

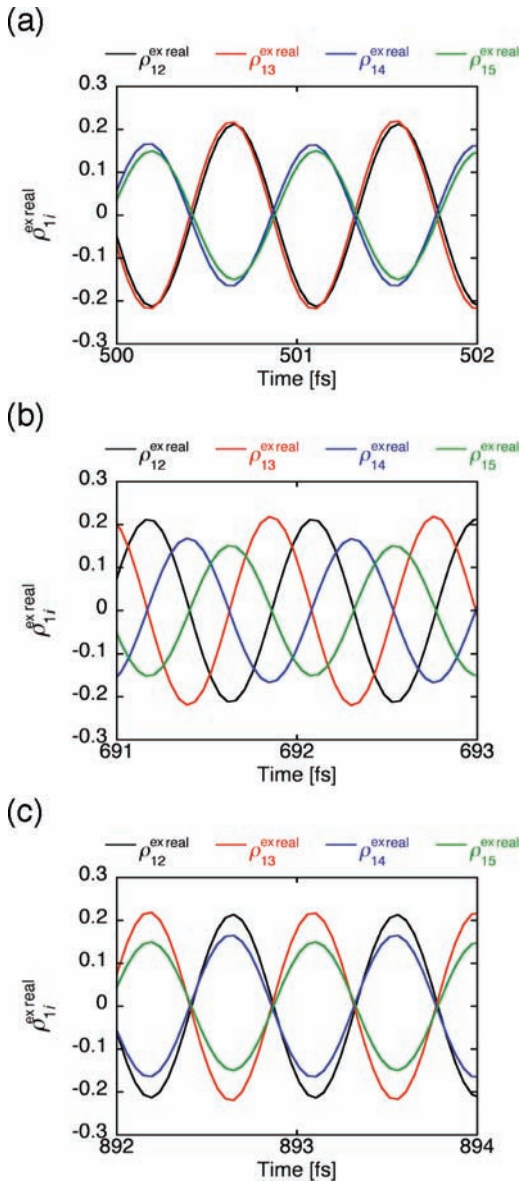

Figure 5. Time evolution of off-diagonal density matrices $\rho_{1i}^{\text{ex real}}(t)$ ($i = 2-5$) at times $t \sim 501$ fs (a), $t \sim 692$ fs (b), and $t \sim 893$ fs (c). See Figure 3 for further legends.

Figure 7 shows the isosurface maps of $\rho_{1i}^{\text{ex real}}(t)d_{1i}(\mathbf{r})$ for $i = 2-5$ at times $t = 501.65$, 692.07, and 892.65 fs. At all times, the spatial distributions of $\rho_{12}^{\text{ex real}}(t)d_{12}(\mathbf{r})$ and $\rho_{15}^{\text{ex real}}(t)d_{15}(\mathbf{r})$ [$\rho_{13}^{\text{ex real}}(t)d_{13}(\mathbf{r})$ and $\rho_{14}^{\text{ex real}}(t)d_{14}(\mathbf{r})$] are found to be similar to each other. Therefore, these two terms contribute to the polarization, electron, and hole densities in the same manner. On the other hand, the relationship between the different types of terms, e.g., $\rho_{12}^{\text{ex real}}(t)d_{12}(\mathbf{r})$ and $\rho_{13}^{\text{ex real}}(t)d_{13}(\mathbf{r})$, is very interesting. As seen from Figure 6, the distributions of $d_{12}(\mathbf{r})$ and $d_{13}(\mathbf{r})$ on the upper side monomer are almost the same, and those on the lower side one are opposite in sign. $\rho_{12}^{\text{ex real}}(t)$ and $\rho_{13}^{\text{ex real}}(t)$ are shown to be in phase at $t = 501.65$ fs (Figure 5a), and thus the contributions of $\rho_{12}^{\text{ex real}}(t)d_{12}(\mathbf{r})$ and $\rho_{13}^{\text{ex real}}(t)d_{13}(\mathbf{r})$ are found to amplify each other on the upper side monomer, but to cancel each other on the lower side monomer (see Figure 7). At $t = 892.65$ fs, $\rho_{12}^{\text{ex real}}(t)$ and $\rho_{13}^{\text{ex real}}(t)$ are shown to be in opposite phase (Figure 5c), so that the contributions of $\rho_{12}^{\text{ex real}}(t)d_{12}(\mathbf{r})$ and $\rho_{13}^{\text{ex real}}(t)d_{13}(\mathbf{r})$ are found to reinforce each other on the lower side monomer, but to diminish each other on the upper side one. In the intermediate time region (around $t = 692.07$ fs), the phase difference between

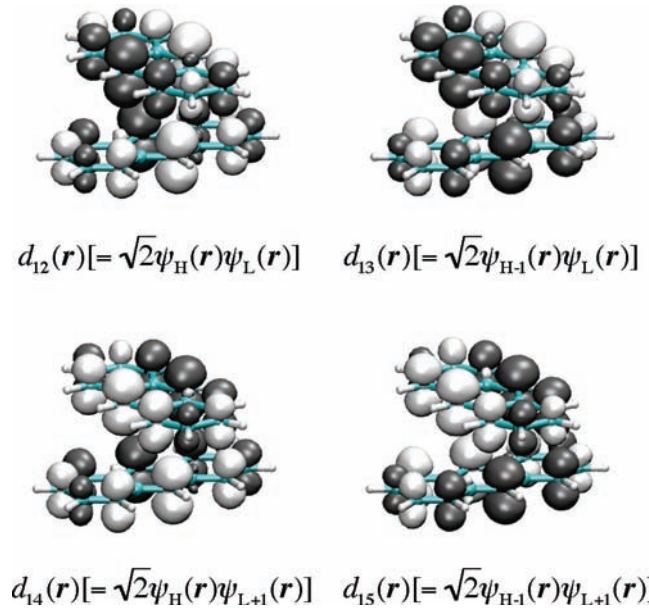

Figure 6. Off-diagonal reduced one-electron density matrices $d_{1i}(\mathbf{r})$ $[=2^{1/2}\psi_a(\mathbf{r})\ \psi_r(\mathbf{r})]$ for $i = 2-5$. White and black surfaces show the isovalue surfaces of ± 0.001 au. See Figure 3 for further legends.

$\rho_{12}^{\text{ex real}}(t)$ and $\rho_{13}^{\text{ex real}}(t)$ is shown to be $\pi/2$ and thus $\rho_{12}^{\text{ex real}}(t)d_{12}(\mathbf{r})$ and $\rho_{13}^{\text{ex real}}(t)\,d_{13}(\mathbf{r})$ contributions appear alternately. In consequence, the spatial distribution of $\sum_{i=2}^{5}\rho_{1i}^{\text{ex real}}(t)d_{1i}(\mathbf{r})$, which is the dominant oscillating part of eqs 5, 7 and 8, shows the slow oscillatory behavior of exciton between the upper and lower side monomers with the frequency of 42 cm^{-1} (a period of about 0.8 ps) accompanied by the rapid oscillations in each monomer. The present result also demonstrates that an exciton recurrence picture in the real model of anthracene dimer is derived from the delocalized ab initio MOs using the dynamic exciton expression in the MOQME approach.

6. Summary

Using the ab initio MO-CI based quantum master equation (MOQME) approach together with a dynamic exciton expression defined by the polarization density, we have clarified the microscopic dynamical behavior of the exciton recurrence motion in a realistic anthracene dimer model after irradiation of a cw laser field. Similarly to the previous studies based on aggregate exciton models, this recurrence motion has been found to be observed when creating a superposition state composed of one-photon allowed two near-degenerate excited states, which involve the excitation configurations with exciton distributions on the both monomers. In the present ab initio approach, we have newly observed there are two characteristic oscillatory behaviors of polarizations: field-induced polarizations with rapid oscillations (with periods corresponding to the excitation energies of the near-degenerate states) and the amplitude oscillation of x- and z-polarization (P^x and P^z) with a slower period. The slower oscillations of P^x and P^z amplitudes are shown to attain maximum alternately with a period corresponding to the slight energy difference between the near-degenerate excited states. From the snapshots of the dynamic exciton expression, these rapid and slow oscillations of polarizations are found to be caused by the polarization in each monomer and the exciton recurrence motion between the monomers, respectively. From the analysis of off-diagonal density matrices, $\rho_{1i}^{\text{ex real}}(t)d_{1i}(\mathbf{r})$, which dominantly describe the oscillatory polarization density, $\rho_{1i}^{\text{real}}(t)$ for $i = 2(\text{H}\rightarrow\text{L})$ and $5(\text{H}-1\rightarrow\text{L}+1)$

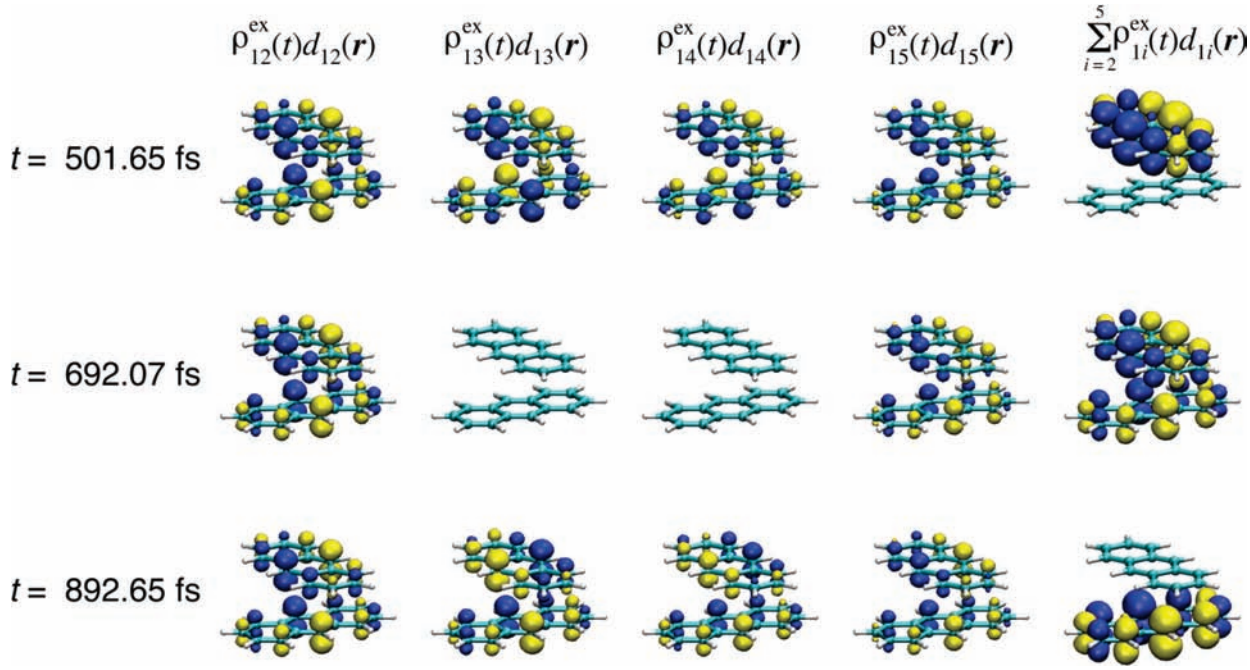

Figure 7. Isosurface maps of $\rho^{ex}_{1i}(t)d_{1i}(\mathbf{r})$ for $i = 2-5$, and of $\sum_{i=2}^{5}\rho^{ex\ real}_{1i}(t)d_{1i}(\mathbf{r})$ at times $t = 501.65$, 692.07, and 892.65 fs. Yellow and blue surfaces show the isovalue surfaces of ± 0.0005 au. See Figure 3 for further legends.

[3(H−1→L) and 4(H→L+1)] are found to oscillate with an eigenfrequency of state **2** (state **3**): there is a difference in oscillation period relating to the energy difference between the two near-degenerate states. Because these frontier MOs of the dimer are constructed from symmetric and antisymmetric mixings of HOMO and LUMO of the monomer with relatively weak coupling, the contributions of $\rho^{real}_{1i}(t)d_{1i}(\mathbf{r})$ turn out to amplify or cancel on each monomer, in which the period of amplification (cancelation) is determined by the difference between the eigenfrequencies of the two near-degenerate states composing a superposition state. As a result, we can illuminate more realistic and detailed dynamic motions of exciton densities composed of both the field-induced rapid polarization oscillations in each monomer and the slower exciton recurrence motion between the monomers using the MOQME approach. Although the present system belongs to a relatively weak intermonomer coupling regime, the advantage of the present approach will be better demonstrated in case of super- and supra-molecular systems with strong couplings and/or delocalized exciton distributions as well as with incoherent (relaxation) effects. The realization of experimental observation of such recurrence behavior strongly depends on the sufficient suppression of the various relaxation effects. In the present MOQME approach, we will discuss the effects of decoherence processes using the relaxation factors $\Gamma_{\alpha\alpha;\beta\beta}$ of eq 2 and $\Gamma_{\alpha\beta;\gamma\delta}$ of eq 3, which are related to the electronic structures through the CI coefficients.[24] The study toward this direction is in progress in our laboratory.

On the other hand, to discuss the coherent energy transfer processes of various real systems, we also need to improve the description of excited states. As is well-known, CIS excitation energy is overshot more than 1 eV. One way to improve this deficiency, the use of time-dependent density functional theory (TDDFT) method is a promising candidate. Although there are still significant problems in conventional DFT exchange-correlation functionals to describe the optical properties, several novel exchange-correlation functionals are developed to overcome the issue. A development of the MOQME method combined with the TDDFT schemes would enable us to perform more quantitative predictions and discussion on the relationships between the electronic structures and coherent processes.

Acknowledgment. This work is supported by Grant-in-Aid for Scientific Research (Nos. 18350007 and 20655003) from Japan Society for the Promotion of Science (JSPS), Grant-in-Aid for Scientific Research on Priority Areas (No. 18066010) from the Ministry of Education, Science, Sports and Culture of Japan, and the global COE (center of excellence) program "Global Education and Research Center for Bio-Environmental Chemistry" of Osaka University.

Supporting Information Available: Movies of exciton dynamics around the three times in Figure 7. All isosurface maps are created using the Virtual Molecular Dynamics (VMD) program.[39] These materials are available free of charge via the Internet at http://pubs.acs.org.

References and Notes

(1) Spano, F. C.; Mukamel, S. *Phys. Rev. A* **1989**, *40*, 5783.
(2) Spano, F. C.; Knoester, J. *Adv. Magn. Opt. Res.* **1994**, *18*, 117.
(3) Ogawa, T.; Tokunaga, E.; Kobayashi, T. *Chem. Phys. Lett.* **2005**, *410*, 18.
(4) Belfield, K. D.; Bondar, M. V.; Hernandez, F. E.; Przhonska, O. V.; Yao, S. *Chem. Phys.* **2006**, *320*, 118.
(5) Ohta, S.; Nakano, M.; Nate, M.; Kishi, R.; Takahashi, H. *Chem. Phys. Lett.* **2007**, *448*, 99.
(6) Devadoss, C.; Bharathi, P.; Moore, J. S. *J. Am. Chem. Soc.* **1996**, *118*, 9635.
(7) Shortreed, M. R.; Swallen, S. F.; Shi, Z.-Y.; Tan, W.; Xu, Z.; Devadoss, C.; Moore, J. S.; Kopelman, R. *J. Phys. Chem. B* **1997**, *101*, 6318.
(8) Kopelman, R.; Shortreed, M.; Shi, Z.-Y.; Tan, W.; Bar-Haim, A.; Klafter, J. *Phys. Rev. Lett.* **1997**, *78*, 1239.
(9) Bar-Haim, A.; Klafter, J.; Kopelman, R. *J. Am. Chem. Soc.* **1997**, *26*, 6197.
(10) Tretiak, S.; Chernyak, V.; Mukamel, S. *J. Phys. Chem. B* **1998**, *102*, 3310.
(11) Harigaya, H. *Phys. Chem. Chem. Phys.* **1999**, *1*, 1687.
(12) Nakano, M.; Takahata, M.; Fujita, H.; Kiribayashi, S.; Yamaguchi, K. *Chem. Phys. Lett.* **2000**, *323*, 249.
(13) Takahata, M.; Nakano, M.; Fujita, H.; Yamaguchi, K. *Chem. Phys. Lett.* **2002**, *363*, 422.

(14) Nakano, M.; Takahata, M.; Yamada, S.; Kishi, R.; Nitta, T.; Yamaguchi, K. *J. Chem. Phys.* **2004**, *120*, 2359.

(15) Ohta, S.; Nakano, M.; Kishi, R.; Takahashi, H.; Furukawa, S.-i. *Chem. Phys. Lett.* **2006**, *419*, 70.

(16) Nakano, M.; Kishi, R.; Nakagawa, N.; Nitta, T.; Yamaguchi, K. *J. Phys. Chem. B* **2005**, *109*, 7631.

(17) Leegwater, J. A.; Durrant, J. R.; Klug, D. R. *J. Phys. Chem. B* **1997**, *101*, 7205.

(18) Takahata, M.; Shoji, M.; Nitta, H.; Takeda, R.; Yamanaka, S.; Okumura, M.; Nakano, M.; Yamaguchi, K. *Int. J. Quantum Chem.* **2005**, *105*, 615.

(19) Kodama, Y.; Ohno, K. *J. Chem. Phys.* **2006**, *125*, 054501.

(20) Kodama, Y.; Ishii, S.; Ohno, K. *J. Phys.: Condens. Matter* **2007**, *19*, 365242.

(21) Akai, I.; Nakao, H.; Kanemoto, K.; Karasawa, T.; Hashimoto, H.; Kimura, M. *J. Lumin.* **2005**, *112*, 449.

(22) Akai, I.; Okada, A.; Kanemoto, K.; Karasawa, T.; Hashimoto, H.; Kimura, M. *J. Lumin.* **2006**, *119/120*, 283.

(23) Minami, T.; Nakano, M.; Fukui, H.; Nagai, H.; Kishi, R.; Takahashi, H. *J. Phys. Chem. C* **2008**, *112*, 16675.

(24) Kishi, R.; Minami, T.; Fukui, H.; Takahashi, H.; Nakano, M. *J. Chem. Phys.* **2008**, *128*, 244306.

(25) Kim, Y. R.; Share, P.; Pereira, M.; Sarisky, M.; Hochstrasser, R. M. *J. Chem. Phys.* **1989**, *91*, 7557.

(26) Zhu, F.; Gralli, C.; Hochstrasser, R. M. *J. Chem. Phys.* **1993**, *98*, 1042.

(27) Matro, A.; Cina, J. A. *J. Phys. Chem.* **1995**, *99*, 2568.

(28) Wynne, K.; Hochstrasser, R. M. *Chem. Phys.* **1993**, *171*, 179.

(29) Wynne, K.; Gnanakaran, S.; Galli, C.; Zhu, F.; Hochstrasser, R. M. *J. Lumin.* **1994**, *60&61*, 735.

(30) Yamazaki, I.; Akimoto, S.; Yamazaki, T.; Sato, S.-i.; Sakata, Y. *J. Phys. Chem. A* **2002**, *106*, 2122.

(31) Yamazaki, I.; Aratani, N.; Akimoto, S.; Yamazaki, T.; Osuka, A. *J. Am. Chem. Soc.* **2003**, *125*, 7192.

(32) Yamazaki, I.; Akimoto, S.; Aratani, N.; Osuka, A. *Bull. Chem. Soc. Jpn.* **2004**, *77*, 1959.

(33) Nitta, H.; Shoji, M.; Takahata, M.; Nakano, M.; Yamaki, D.; Yamaguchi, K. *J. Photochem. Photobiol. A: Chem.* **2006**, *178*, 264.

(34) Nakano, M.; Ohta, S.; Kishi, R.; Nate, M.; Takahashi, H.; Furukawa, S.-i.; Nitta, H.; Yamaguchi, K. *J. Chem. Phys.* **2006**, *125*, 234707.

(35) Carmichael, H. J. *Statistical Methods in Quantum Optics 1*; Springer: Verlag, Berlin, 1999.

(36) Haken, H. *Quantenfeldtheorie des Festkörpers*; B. G. Teubner: Stuttgart, 1973.

(37) Nakano, M.; Kishi, R.; Minami, T.; Fukui, H.; Nagai, H.; Yoneda, K.; Takahashi, H. *Chem. Phys. Lett.* **2008**, *460*, 370.

(38) Frisch, M. J.; Trucks, G. W.; Schlegel, H. B.; Scuseria, G. E.; Robb, M. A.; Cheeseman, J. R.; Montgomery, Jr. J. A.; Vreven, T.; Kudin, K. N.; Burant, J. C.; Millam, J. M.; Iyengar, S. S.; Tomasi, J.; Barone, V.; Mennucci, B.; Cossi, M.; Scalmani, G.; Rega, N.; Petersson, G. A.; Nakatsuji, H.; Hada, M.; Ehara, M.; Toyota, K.; Fukuda, R.; Hasegawa, J.; Ishida, M.; Nakajima, T.; Honda, Y.; Kitao, O.; Nakai, H.; Klene, M.; Li, X.; Knox, J. E.; Hratchian, H. P.; Cross, J. B.; Bakken, V.; Adamo, C.; Jaramillo, J.; Gomperts, R.; Stratmann, R. E.; Yazyev, O.; Austin, A. J.; Cammi, R.; Pomelli, C.; Ochterski, J. W.; Ayala, P. Y.; Morokuma, K.; Voth, G. A.; Salvador, P.; Dannenberg, J. J.; Zakrzewski, V. G.; Dapprich, S.; Daniels, A. D.; Strain, M. C.; Farkas, O.; Malick, D. K.; Rabuck, A. D.; Raghavachari, K.; Foresman, J. B.; Ortiz, J. V.; Cui, Q.; Baboul, A. G.; Clifford, S.; Cioslowski, J.; Stefanov, B. B.; Liu, G.; Liashenko, A.; Piskorz, P.; Komaromi, I.; Martin, R. L.; Fox, D. J.; Keith, T.; Al-Laham, M. A.; Peng, C. Y.; Nanayakkara, A.; Challacombe, M.; Gill, P. M. W.; Johnson, B.; Chen, W.; Wong, M. W.; Gonzalez, C.; Pople, J. A. *Gaussian 03*, Revision C.02, Gaussian, Inc.: Wallingford CT, 2004.

(39) Humphrey, W.; Dalke, A.; Schulten, K. *J. Mol. Graph.* **1996**, *14*, 33.

JP8111588